

## EXPLORING THE ECO-FRIENDLY SYNTHESIS OF IRON NANOPARTICLES FROM VERNONIA CINERIA: ASSESSING ANTIMICROBIAL EFFICACY AND PHOTODEGRADATION CAPABILITIES

Mary Jency. J<sup>1</sup>, Dr. S.R. Brintha<sup>2\*</sup>

Reg.No: 20113012032001

<sup>1,2\*</sup>Department of Chemistry, Annai Velankanni College, Tholayavattam, Kanyakumari District Tamil Nadu.

Affiliated to Manonmaniam Sundaranar University, Tirunelveli- 627 012.

\*Corresponding Author: Dr. S.R. Brintha

### Abstract

The utilization of biological and environmentally friendly synthesis processes presents a promising alternative to conventional physico-chemical methods. This study explores the potential of leveraging biological entities such as plants, fungi, and bacteria in the synthesis of iron nanoparticles, highlighting the efficacy of green techniques in nanoparticle production. Specifically, this study demonstrates the use of *Vernonia cineria* leaf extract for the generation of iron nanoparticles, showcasing its multifunctional role as surface stabilizers, capping agents, and reducing agents. Iron nanoparticles from *V. cineria* leaf extract characterization by UV visible spectroscopy, FTIR, XRD, SEM and EDAX. Antibacterial and antifungal assays demonstrated the efficient activity of iron nanoparticles against pathogens, indicating potential biomedical applications. The photodegradation experiments highlighted the photocatalytic potential of iron nanoparticles, with degradation efficiency improving over time. The substantial percentage of degradation achieved within the first 120 minutes underscores the effectiveness of the degradation process under the experimental conditions. Future research should further explore the potential applications of iron nanoparticles synthesized from *V. cineria* extract and investigate their environmental and biomedical implications.

**Keywords:** *Vernonia cineria*, iron nanoparticles, characterization, antibacterial assay, antifungal assay, photodegradation activity.

### 1. Introduction

Nanotechnology has evolved as a ground-breaking discipline that has practical applications in a variety of fields, including medicine and environmental remediation. In recent years, there has been a growing interest in environmentally friendly ways of synthesis, which has led to the investigation of green methodologies that make use of natural sources such as plants. There are a number of factors that have a significant impact on the physicochemical properties of the nanoparticles that have been synthesized. These include the reaction conditions, which include the concentration of metal precursors, the amount of plant extract that is involved in the reaction, the reaction temperature, and the reaction time, as well as the properties of the plant extract, which include the pH, antioxidant capacity, extract concentration and the time and temperature at which the extract is prepared (Ebrahiminezhad *et al.*, 2016).

Because of their diminutive size, nanoparticles possess unusual physical and chemical characteristics. As a result, they are very desired for use in a variety of applications, including those in the domains of medicine, electronics and catalysis. Given their huge surface area-to-volume ratio and the fact that their characteristics may be tuned, they provide a tremendous opportunity for innovation and improvement across a wide range of sectors. In spite of the fact that physical and chemical methods have the potential to successfully produce nanoparticles that are both pure and well-specified, they are not economically

sustainable and typically call for a significant amount of equipment serving as a natural source for reducing and capping agents in a one-pot synthesis reaction. This eliminates the problems associated with multistep synthesis practices and the expenses associated with chemical reagents (Dinali *et al.*, 2017). Green synthesis, which calls for the use of natural sources as reducing and stabilizing agents, provides an alternative to standard techniques of nanoparticle synthesis that is more environmentally friendly. This method not only lessens the negative effects that the creation of nanoparticles has on the environment, but it also opens up the possibility of developing more environmentally friendly manufacturing techniques.

Among the natural sources that have been examined for green synthesis, plants stand out owing to the number of phytochemicals that they contain and have a rich phytochemical makeup. Plant-mediated synthesis has garnered a significant amount of scientific attention among the many biological systems that have been established (Makarov *et al.*, 2014). Within the scope of this investigation, we investigate the process of synthesising nanoparticles by using plant extracts as reducing and holding agents. Particularly, we are looking at the possibility of using *Vernonia cineria* extract in the environmentally friendly production of iron nanoparticles at this time. Our objective is to get a better understanding of the effectiveness, stability and possible uses of these biogenic nanoparticles by conducting in-depth characterization and analytical activities. *V. cineria*, commonly known as "Sahadevi" or "Sahadeva," is a medicinal plant widely distributed in tropical and subtropical regions. It belongs to the family Asteraceae. Various parts of *V. cineria* have been traditionally used in folk medicine for their therapeutic properties. Despite the fact that there were not many research that discussed the synthesis of iron nanoparticles from *V. cineria*, the extracts of *V. cineria* were successful in achieving a green synthesis of silver (Ramaswamy *et al.*, 2015), zinc oxide (Azim *et al.*, 2022), nickel (Chauhan *et al.*, 2023) and gold nanoparticles (Singh *et al.*, 2021).

Therefore, considering the important of the above in the present studies have shown that synthesized of iron nanoparticle form *V. cineria* extract. The synthesized nano particles were characterised by UV visible spectroscopy, FTIR, XRD, SEM and EDAX and screening of their extracts are efficient against both gram-positive and gram-negative bacteria. These extracts have been discovered to impede the proliferation of pathogens such as *Staphylococcus aureus*, *Escherichia coli*, *Pseudomonas aeruginosa*, *Staphylococcus aureus*, *Klebsiella pneumoniae*, *Enterococcus faecalis* and *Proteus vulgaris*. Moreover, synthesized nano particles derived from *V. cineria* have shown encouraging antifungal properties against many fungal species, such as *Aspergillus niger*, *Aspergillus flavus* and *Candida albicans*. The antifungal effectiveness of *V. cineria* makes it a promising choice for treating fungal infections in both people and plants. hotodegradation activity of *V. cineria* extract holds promise for environmental remediation applications, particularly in the treatment of water and soil contaminated with organic pollutants.

## 2. Methodology

### 2.1. Preparation of leaf extract and biosynthesis of iron nanoparticles

*V. cineria* were gathered from Saral, Kanyakumari district, Tamilnadu. The authentication of the plant was done by Dr. Nagendra Prasad, Botanist, Retd Professor, Sri Paramakalyani College, Alwarkurichi. The leaves were rinsed with tap water and extracts were prepared. Leaf extracts were prepared by taking around 25 grams of leaves. The samples were carefully cleansed with distilled water, then dried and pulverized using a mixer. Finally, they were finely homogenized using a mortar and pestle. 2gm of plant extract was dissolved in 50ml of ethanol, hexane, chloroform and deionized water and stirred with a magnetic stirrer for three hours to get *V. cinerea* plant extract. The aqueous *V. cineria* extract was filtered after an hour of stabilization. 10ml of 0.01 M FeSO<sub>4</sub> solution at 70°C was mixed with the filtrate. The solution was chilled and centrifuged at 10,000 rpm for 2 min. The product was dried in an oven at

50°C for 3 hours which led to the synthesis of iron nanoparticles (Vc-FeNPs).

## 2.2. Characterization of iron nanoparticles

The size, elemental composition and morphology of FeNPs in *V. cineria* are analyzed using analytical methods such as UV-visible spectrophotometry (UV-Vis), Fourier Transform Infrared Spectroscopy (FTIR), Xray Diffraction analysis (XRD) and SEM-EDAX (Scanning Electron Microscope equipped with Energy Dispersive Xray analysis).

## 2.3. Antimicrobial Activity

### 2.3.1. Test organisms

*Escherichia coli*, *Bacillus subtilis*, *Staphylococcus aureus*, *Klebsiella pneumoniae*, *Enterococcus faecalis*, *Proteus vulgaris*, *Aspergillus niger*, *Aspergillus flavus* and *Candida albicans* were bought from MTCC Chandigarh for antimicrobial analysis.

### 2.3.2. Determination of Antibacterial Activity

Nutrient Agar (NA) was employed for bacteria and Sabouraud Dextrose Agar (SDA) for fungi. Pure culture from the plate was subcultured on nutrient agar and SDA agar at 37°C and 22°C for 24- 48hrs. To make a  $1.5 \times 10^8$  cfu/ml bacterial solution, human pathogenic bacterial strains individually grown in nutrient broth at 37°C for 24hrs. For the medium, 38 g Mueller-Hinton Agar Medium (Hi Media) was dissolved in 1000ml distilled water. Under 15 Lbs pressure at 121°C (pH 7.3), the dissolved medium was autoclaved for 15 min. The autoclaved media was mixed and put on 25 ml Petri plates after cooling. The bacterial culture were spread over nutrient agar plate. About 60-80 µl of Vc-FeNPs extract were applied in a emty sterile disc (10mm). Positive control was streptomycin 10 mcg disc and negative control was empty sterile disc. Plates were incubated at 37°C for 24 hrs and growth of inhibition zones were recorded. The disc's inhibitory zones were measured in millimeters using a transparent ruler after incubation.

### 2.3.3. Determination of Antifungal Activity

The fungal *Aspergillus niger*, *Aspergillus flavus* and *Candida albicans* were spread over on SDA agar with the help of a swab. Up to 80 µl of Vc-FeNpS extract concentration were added on a sterile disc (10mm) using a pipette. For the positive control, a 10 mm sterile disc was filled with 150 mcg fluconazole, while the negative control was empty sterile disc. Place the disc on SDA medium and let the compound diffuse for 5 minutes. Incubate the plates at 22°C for 48 hours. After incubation the plates were examined for growth inhibition of test fungal pathogen through zone of inhibition and the diameter of the zone of inhibition was measured and recorded.

## 2.4. Photodegradation Activity

The photocatalytic activity of Vc-FeNPs was tested for methylene blue dye degradation in sunlight and at different irradiation times. Vc-FeNPs sample (0.1 g) was added into 100ml of 10mg/l methyleneblue dye at constant temperature. To reach equilibrium, the catalyst and dye solution were stirred in a dark magnetic stirrer. After the attachment of the equilibrium, dye-sample solutions were photodegraded by sun light. To remove catalyst particles, 5ml of solution was centrifuged at different time interval (0- 120 min). Absorbance of withdrawn solutions was measured at 664nm using UV-visible spectrophotometer.

## 3. Result

The iron nanoparticles were successfully synthesized in a easy and eco-friendly way using the *V. cineria* leaves extract. The FeSO<sub>4</sub> solution was added to the *V. cineria* extract. The colour changing ( Fig. 1 ) confirmed the production of iron nano particles.



**Fig. 1: Bio synthesised of Iron nanoparticles from *Vernonia cineria***

### 3.1. Characterizations

Prepared Vc-FeNPS were analysed by UV visible spectroscopy, FTIR, XRD, SEM and EDAX.

#### 3.1.1. UV of ethanol extract of *Vernonia cineria*

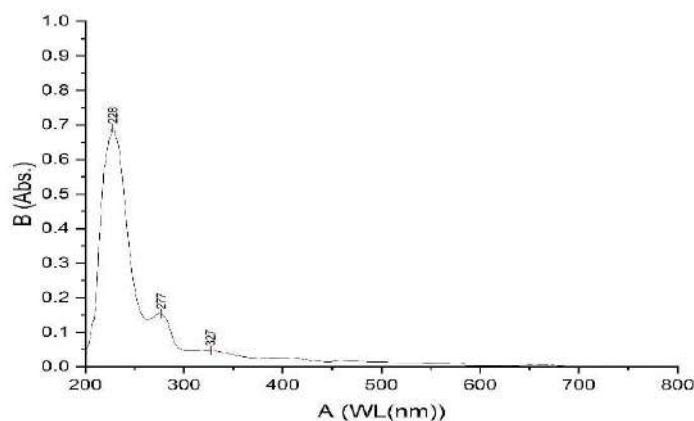


**Fig. 2: UV of ethanol extract of *Vernonia cineria***

The maximum absorption spectra of an ethanol extract of *V. cineria* fall at 228nm, 277nm, and 327nm can be attributed to the presence of specific chromophores and functional groups within the molecules present in the extract is shown in Fig 2. The absorption at 228 nm is most likely attributed to substances such as flavonoids, phenolic acids, or specific alkaloids. These compounds are well-known for their ability to absorb light in the UV range. The presence of a peak at 277nm indicates the existence of aromatic compounds, such as flavonoids, lignans, or other polyphenolic compounds. These compounds usually absorb light around this wavelength due to the presence of aromatic rings. At 327nm, the absorption can be linked to compounds that possess conjugated double bonds or extended  $\pi$ -electron systems. These compounds are commonly found in polyphenolic compounds, flavonoids, and other plant metabolites.

### 3.1.2. UV of hexane extract of *Vernonia cineria*

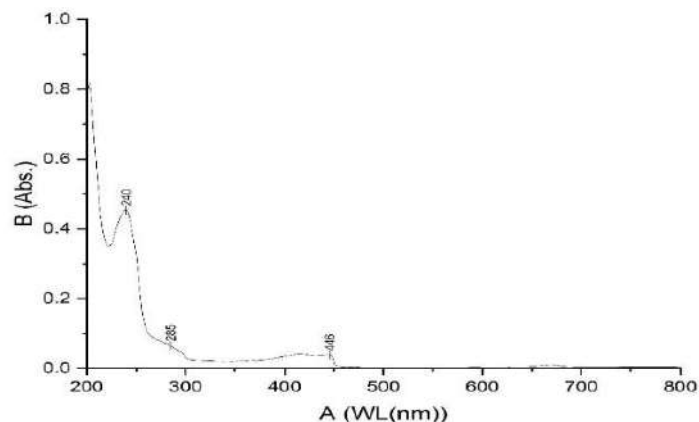


**Fig. 3:** UV of hexane extract of *Vernonia cineria*

The maximum absorption spectra of an hexane extract of *V. cineria* shows 240nm the presence of conjugated double bonds or aromatic rings detected, indicating compounds like terpenoids, steroids or lipophilic substances (Fig. 3). 285nm indicates the presence of functional groups such as carbonyl groups in compounds like ketones, aldehydes or unsaturated fatty acids and 446nm corresponds to absorption peak of certain pigments or polyenes present in the extract, potentially indicating the presence of compounds like carotenoids or other polyene chains, which often absorb light in the visible range.

### 3.1.3. UV of chloroform extract of *Vernonia cineria*

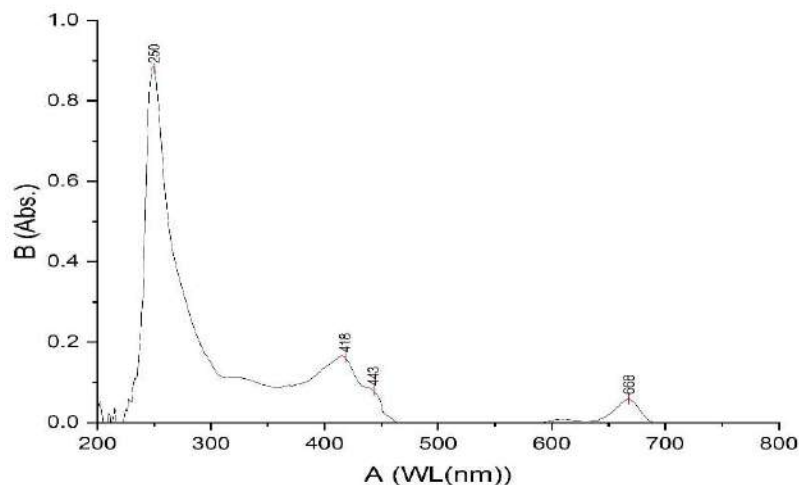


**Fig.4:** UV of chloroform extract of *Vernonia cineria*

The maximum absorption spectra of an chloroform extract of *V. cineria* shows 250nm indicates the presence of conjugated double bonds or aromatic rings in compounds such as flavonoids, terpenoids, or other polyphenolic substances whereas 418nm shows the presence of certain flavonoids, anthocyanins, or other polyphenolic compounds. 443nm corresponds to the absorption peak of certain pigments or polyenes present in the extract, such as carotenoids or other polyene chains. Compounds with conjugated double bonds often absorb light in the visible range, and a peak at 443nm could signify their presence. 668nm could be indicative of specific chlorophyll derivatives or other chloroplast pigments

present in the extract (Fig.4).

### 3.1.4. UV of Iron nanoparticles synthesised from *Vernonia cineria*

UV- visible spectra showed that maximum nano particles synthesis was obtained in the case of 10ml of *V. cineria* plant extract solution (Fig 5). As a result, two absorption peaks at the wavelength of 268nm and 347nm showed the presence of iron nanoparticles. Absorption at 268nm indicates the likely presence of smaller iron nanoparticles or iron oxide nanoparticles. Such nanoparticles typically display UV absorption due to electronic transitions occurring within their structures. Conversely, the presence of larger iron nanoparticles or aggregates is suggested by absorption at 347nm. As iron nanoparticle size increases, their absorption spectrum tends to extend into the visible region, potentially resulting in a peak at 347nm.

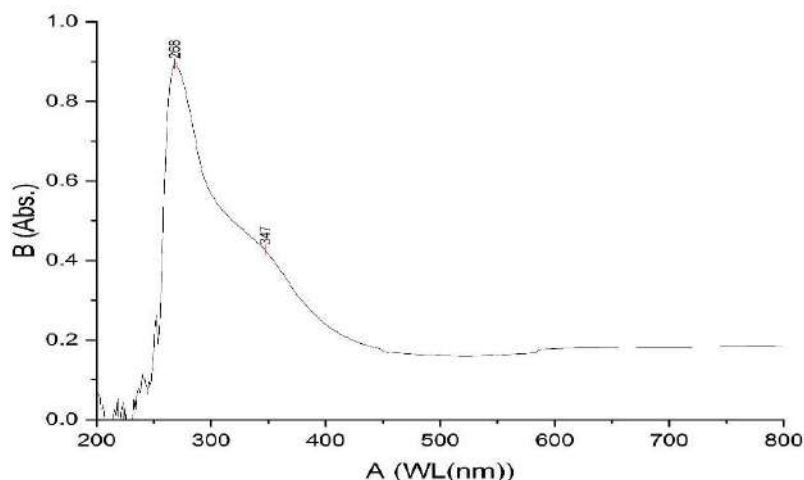


Fig. 5: UV of Iron nanoparticles synthesised from *Vernonia cineria*

### 3.1.5. FTIR of ethanol extract of *Vernonia cineria*

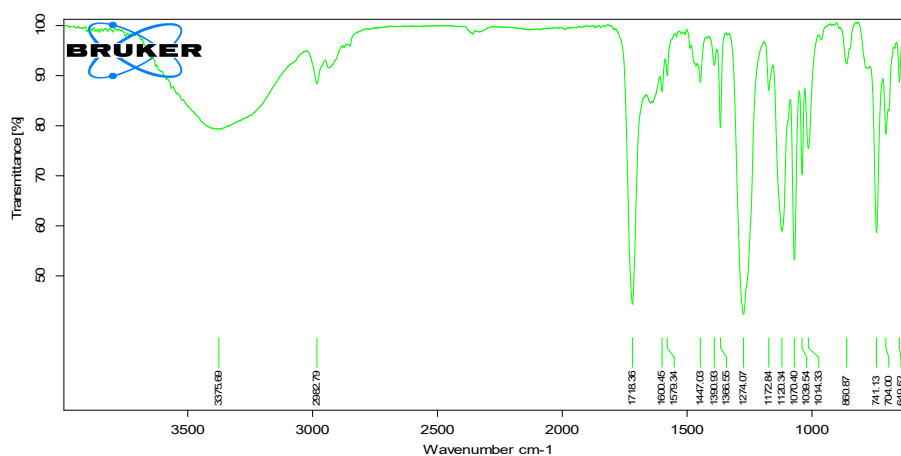


Fig 6: FTIR of ethanol extract of *Vernonia cineria*

**Table 1: FTIR of ethanol extract of *Vernonia cineria***

| Wave length | Functional groups | Structure                        |
|-------------|-------------------|----------------------------------|
| 649.52      | Alkyl halides     | R-Br                             |
| 704.00      | Aromatics         | monosubst                        |
| 741.13      | Aromatics         | 1,2,3-trisub                     |
| 860.87      | Misc.             | S-OR esters                      |
| 1014.33     | Alkyl halides     | R-F                              |
| 1039.54     | Amines            | R <sub>2</sub> NH                |
| 1070.40     | Amines            | RNH <sub>2</sub>                 |
| 1120.34     | Alkyl halides     | R-F                              |
| 1172.84     | Alkyl halides     | R-F                              |
| 1274.84     | Amines            | Ar <sub>2</sub> NH               |
| 1366.55     | Alkanes           | C-H rock                         |
| 1390.93     | Misc.             | S=O sulfate                      |
| 1447.03     | Aromatics         | C-C in ring                      |
| 1579.34     | Amines            | RNH <sub>2</sub>                 |
| 1600.45     | Amides            | RCONH <sub>2</sub>               |
| 1718.36     | Ketones           | R <sub>2</sub> CO                |
| 2982.79     | Alkanes           | RCH <sub>2</sub> CH <sub>3</sub> |
| 3375.69     | Carboxylic acids  | RCO-OH                           |

The FTIR spectrum of ethanol extract of *V. cineria* showed in Fig. 6 respectively. In this figure showed broadest peak at 3375cm<sup>-1</sup> which corresponds to the carboxylic acids, whereas the sharp peaks at 1718cm<sup>-1</sup> and 1274cm<sup>-1</sup> shows the presence of ketones and amines. Other sharp peaks at 1120cm<sup>-1</sup>, 1070cm<sup>-1</sup>, 1014cm<sup>-1</sup>, 1039cm<sup>-1</sup> and 741cm<sup>-1</sup> associates with the presence of alkyl halides, amines and aromatics respectively. Alkanes, amides, amines, aromatics, misc, alkanes, alkyl halides were also seen in the peaks formed at 2982cm<sup>-1</sup>, 1600cm<sup>-1</sup>, 1579cm<sup>-1</sup>, 1447cm<sup>-1</sup>, 1390cm<sup>-1</sup>, 1366cm<sup>-1</sup> and 1172cm<sup>-1</sup> which were neither broad nor sharp.

### 3.1.6. FTIR of hexane extract of *Vernonia cineria*

The strong sharp bands at  $2922\text{cm}^{-1}$  and  $2852\text{cm}^{-1}$  in the hexane extract of *V. cineria* corresponds to the alkanes group and  $1727\text{cm}^{-1}$  associates with aldehydes. Other bands at  $3412\text{cm}^{-1}$ ,  $1461\text{cm}^{-1}$ ,  $1377\text{cm}^{-1}$ ,  $1267\text{cm}^{-1}$ ,  $1169\text{cm}^{-1}$ ,  $1100\text{cm}^{-1}$ ,  $1079\text{cm}^{-1}$ ,  $1046\text{cm}^{-1}$  and  $969\text{cm}^{-1}$  corresponds to the phenols, alkanes, amines, alkyl halides, alcohols, ethers and amides, as shown in Fig 7.

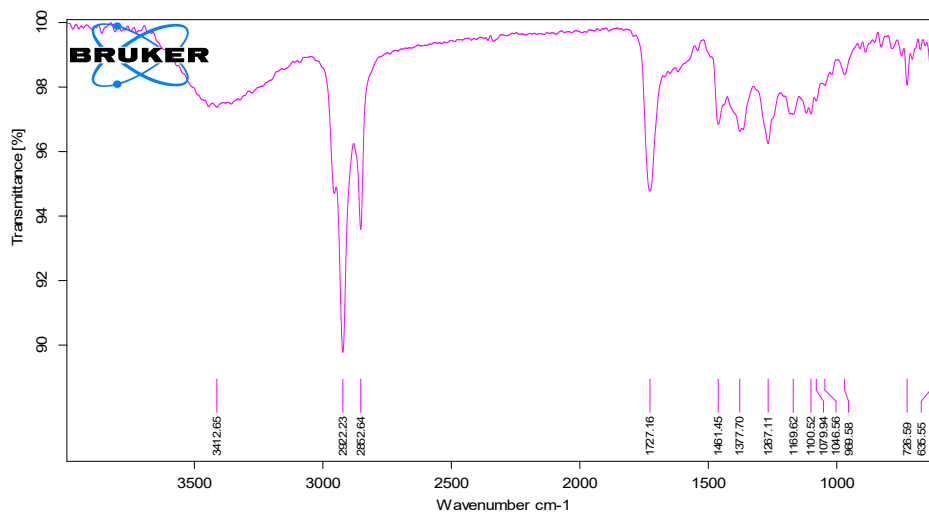


**Fig. 7: FTIR of hexane extract of *Vernonia cineria***

**Table 2: FTIR of hexane extract of *Vernonia cineria***

| Wave length | Functional groups | Structure                  |
|-------------|-------------------|----------------------------|
| 613.95      | Alkynes           | $\text{RC}\equiv\text{CH}$ |
| 635.55      | Alkynes           | $\text{RC}\equiv\text{CH}$ |
| 726.59      | Misc.             | S-OR esters                |
| 969.58      | Alkenes           | $\text{cisRCH}=\text{CHR}$ |
| 1046.56     | Alcohols          | $\text{RCH}_2\text{OH}$    |
| 1079.94     | Ethers            | $\text{R-O-R}$             |
| 1100.52     | Alcohols          | $\text{R}_2\text{CHOH}$    |
| 1169.62     | Alkyl halides     | $\text{R-F}$               |
| 1267.11     | Amines            | $\text{Ar}_2\text{NH}$     |
| 1377.70     | Alkanes           | $\text{RCH}_2\text{CH}_3$  |
| 1461.45     | Alkanes           | $\text{RCH}_2\text{CH}_3$  |
| 1727.16     | Aldehydes         | $\text{RCHO}$              |
| 2852.64     | Alkanes           | $\text{RCH}_2\text{CH}$    |
| 2922.23     | Alkanes           | $-\text{CH}_2-$            |
| 3412.65     | Phenols           | $\text{Ar O-H bonded}$     |



### 3.1.7. FTIR of chloroform extract of *Vernonia cineria*

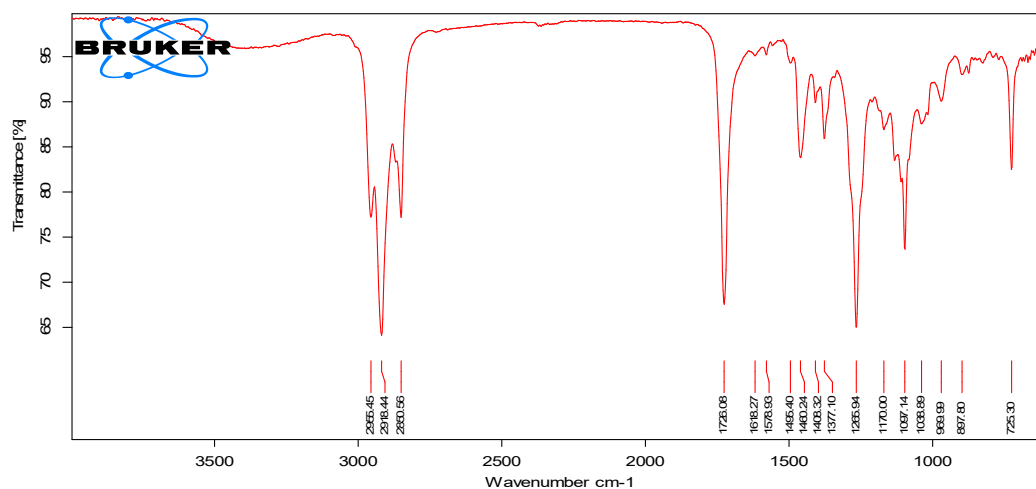


**Fig. 8: FTIR of chloroform extract of *Vernonia cineria***

**Table 3: FTIR of chloroform extract of *Vernonia cineria***

| Wave length | Functional groups | Structure                        |
|-------------|-------------------|----------------------------------|
| 725.30      | Alkanes           | RCH <sub>2</sub> CH <sub>3</sub> |
| 897.80      | Misc.             | S-OR esters                      |
| 969.99      | Alkenes           | Cis RCH=CHR                      |
| 1038.89     | Alkyl halides     | RF                               |
| 1097.14     | Amines            | R <sub>2</sub> NH                |
| 1170.00     | Amines            | RNH <sub>2</sub>                 |
| 1265.94     | Alkyl halides     | CH <sub>2</sub> χ                |
| 1377.10     | Alkanes           | RCH <sub>2</sub> CH <sub>3</sub> |
| 1408.32     | Aromatics         | C-C in ring                      |
| 1460.24     | Alkanes           | RCH <sub>2</sub> CH <sub>3</sub> |
| 1726.08     | Aldehydes         | RCHO                             |
| 2850.56     | Alkanes           | -CH <sub>2</sub> -               |
| 2918.44     | Alkanes           | RCH <sub>2</sub> CH              |
| 2955.45     | Alkanes           | RCH <sub>2</sub> CH <sub>3</sub> |

The sharp bands at 2955cm<sup>-1</sup>, 2918cm<sup>-1</sup>, 2850cm<sup>-1</sup>, 1460cm<sup>-1</sup> and 725cm<sup>-1</sup> in the chloroform extract of *V. cineria* corresponds to the presence of alkanes and 1726cm<sup>-1</sup> represents aldehydes. 1265cm<sup>-1</sup> and 1038cm<sup>-1</sup> are other sharp peaks that associate with alkyl halides. Weak bands at 1408cm<sup>-1</sup>, 1377cm<sup>-1</sup>, 1170cm<sup>-1</sup>, 1096cm<sup>-1</sup> and 969cm<sup>-1</sup> represents the presence of aromatics, alkanes and amines was shown in Figure 8.

### 3.1.8. FTIR of iron nanoparticles from *Vernonia cineria*

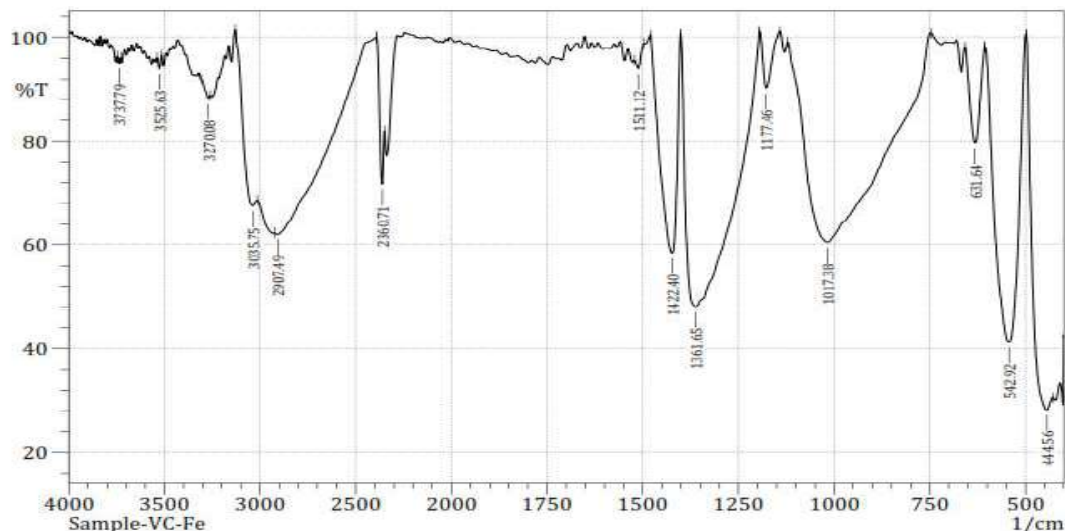


Fig.9: FTIR of iron nanoparticles from *Vernonia cineria*

Table 4: FTIR of iron nanoparticles from *Vernonia cineria*

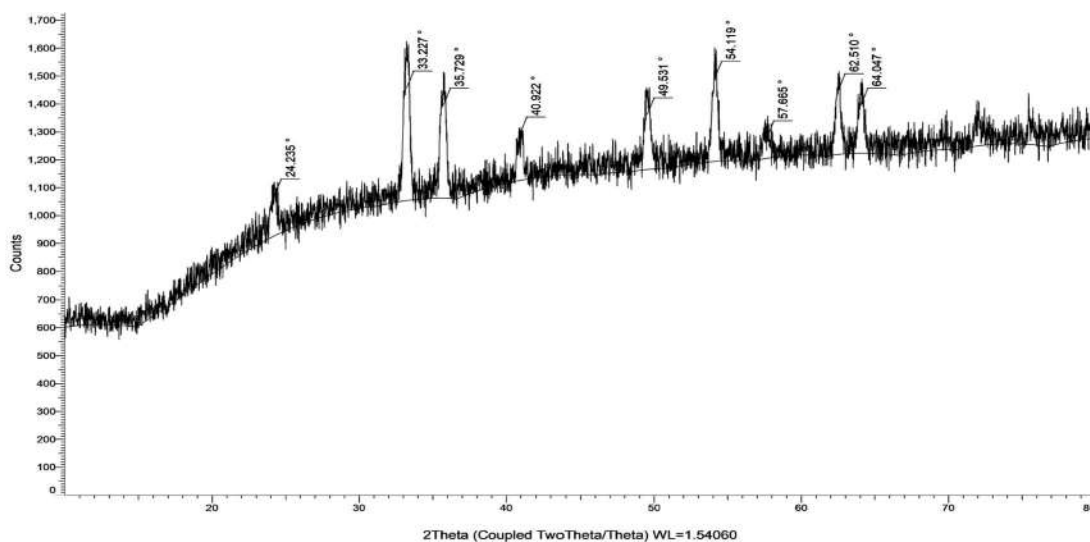
| Wave length | Functional groups | Structure           |
|-------------|-------------------|---------------------|
| 444.56      | Misc.             | S-S disulfide       |
| 542.92      | Alkyl halides     | R-Br                |
| 631.64      | Alkynes           | RC#CH               |
| 1017.38     | Carboxylic acids  | RCO-OH              |
| 1177.46     | Alkyl halides     | R-F                 |
| 1360.65     | Amines            | Ar <sub>2</sub> NH  |
| 1422.40     | Aromatics         | C-C in ring         |
| 1511.12     | Misc.             | N=O nitroso         |
| 2360.71     | Misc.             | P-H phosphine       |
| 2907.49     | Carboxylic acids  | C=C-CO-OH           |
| 3035.75     | Aromatics         | Ar-H                |
| 3270.08     | Alkynes           | RC#C-H              |
| 3525.63     | Alcohols          | RCH <sub>2</sub> OH |
| 3737.79     | Alcohols          | R <sub>2</sub> CHOH |

Fig 9. Shows FTIR spectra of iron nanoparticles show strong bands at  $2907\text{ cm}^{-1}$ ,  $1422\text{ cm}^{-1}$ ,  $1360\text{ cm}^{-1}$ ,  $1017\text{ cm}^{-1}$  and  $542\text{ cm}^{-1}$  corresponds to carboxylic acids, aromatics, amines.  $2360\text{ cm}^{-1}$ ,  $631\text{ cm}^{-1}$  and  $444\text{ cm}^{-1}$  are other sharp peaks that associate with Misc. The absence of specific peaks observed in the plant extracts suggests a transformation of functional groups during the synthesis process, possibly due to the involvement of plant-derived compounds in the reduction and stabilization of iron nanoparticles.

### 3.1.8. XRD of iron nanoparticles from *Vernonia cineria*

The composition of the synthesized iron oxide powder was analyzed using (XRD, Bruker D8 Advance). The XRD results obtained were compared with the X-ray data file from the Joint Committee on Powder Diffraction Standards (JCPDS) (Fig 10). The XRD of FeNPs synthesized using leaf extract of *V.*

*cineria*. A number of strong bragg's reflection with peaks were observed at specific angles at room temperature:  $2\theta$  value of  $24.23^\circ$ ,  $33.22^\circ$ ,  $35.72^\circ$ ,  $40.92^\circ$ ,  $49.53^\circ$ ,  $54.11^\circ$ ,  $57.66^\circ$ ,  $62.51^\circ$ , and  $64.04^\circ$  respectively. The Scherrer relation was used in order to determine the crystallite size of the nanoparticles. This was accomplished by measuring the broadening of the XRD peaks of the preferred orientation. The average crystallite size was found to be 53nm.



**Fig. 10: XRD of iron nanoparticles from *Vernonia cineria***

### 3.1.9. SEM and EDAX of iron nanoparticles from *Vernonia cineria*

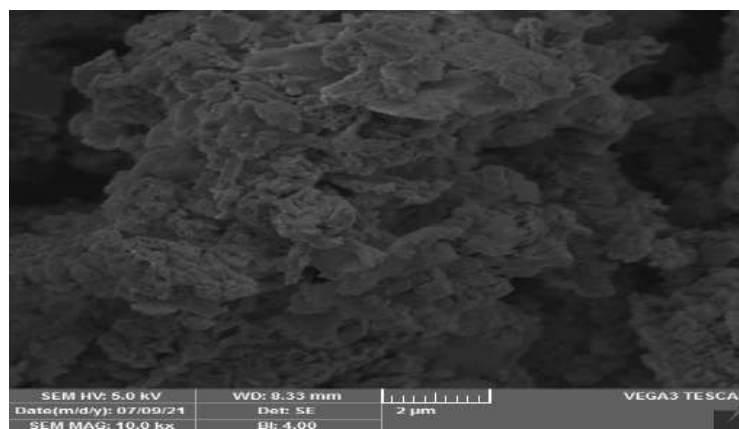


**Fig. 11: SEM of iron nanoparticles from *Vernonia cineria***

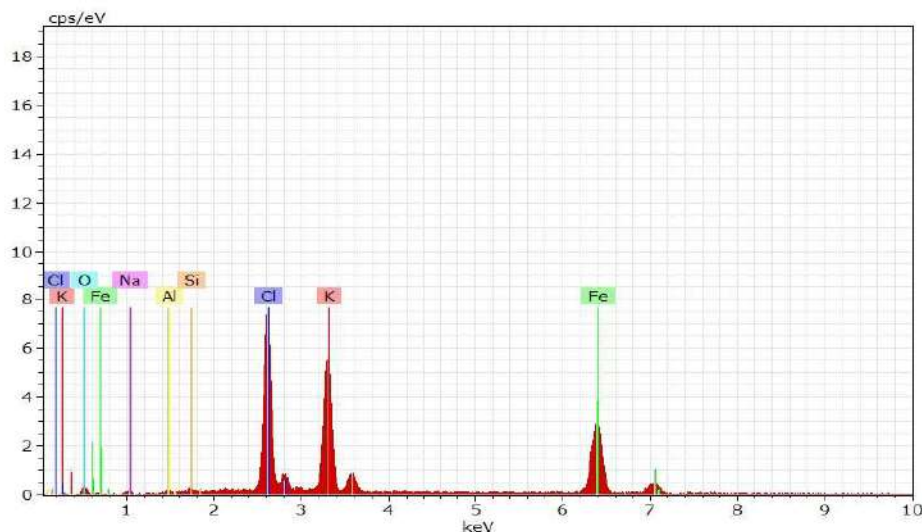


**Fig. 12: EDAX of iron nanoparticles from *Vernonia cineria***

Thus the surface morphology and size of the silver nanoparticles were analyzed by SEM. Based on the analysis of the SEM image, it can be observed that the nanoparticles exhibited a size distribution ranging from 50-60nm. Fig.11 showed that the particles are spherical in shape and aggregates into larger particles which are of different sizes. This is in agreement with the size obtained from the Deybe Scherrer equation. An EDAX examination is conducted to ascertain the composition of iron oxide nanoparticles. EDAX analysis has shown the formation of pure iron oxide nanoparticles.

### 3.1.10. Antibacterial activity of iron nanoparticles from *Vernonia cineria*

**Table 5: Antibacterial activity of *Vernonia cineria* mediated Iron nanoparticles**

| Sample                  | <i>E. coli</i> | <i>B. subtilis</i> | <i>S. aureus</i> | <i>K. pneumoniae</i> | <i>E. faecalis</i> | <i>P. vulgaris</i> |
|-------------------------|----------------|--------------------|------------------|----------------------|--------------------|--------------------|
| Vc-FeNps                | 20 mm          | 14 mm              | 13 mm            | 13 mm                | 14 mm              | NZ                 |
| + <sup>ve</sup> control | 24 mm          | 21 mm              | 21 mm            | 15 mm                | 21 mm              | 16 mm              |
| - <sup>ve</sup> control | NZ             | NZ                 | NZ               | NZ                   | NZ                 | NZ                 |

Iron nanoparticles synthesised from *Vernonia cineria* was tested for antimicrobial activity against bacterial culture such as *Escherichia coli*, *Bacillus subtilis*, *Staphylococcus aureus*, *Klebsiella pneumoniae*, *Enterococcus faecalis* and *Proteus vulgaris* (Plate.2). The nanoparticles showed maximum activity of around 20mm of zone of inhibition against *E.coli* which is closer to the positive control that has 24mm of zone. *B. subtilis* and *E. faecalis* was observed with a zone of inhibition of 14mm whereas the positive control showed 21mm of zones. The minimum of 13mm of zones were observed with *S. aureus* and *K. pneumoniae* the positive control has a zone of inhibition of 21mm against *S. aureus* and 15mm against *K. pneumoniae*. No zones were noticed in the plate that was incubated with *P. vulgaris* that says there was no activity whereas the positive control showed 16mm of zone against *P. vulgaris* (Table. 5). Antifungal activity was tested against three pathogens *Aspergillus niger*, *Aspergillus flavus* and *Candida albicans* (Plate.3). Iron nanoparticles showed with 13mm, 12mm and 10mm of the zone of inhibition was obtained against *A. niger*, *A. flavus* and *C. albicans* which is lesser than the positive control that showed zones of 21mm for *A. niger* and *A. flavus* as well as 16 mm of zones of inhibition

against *C. albicans* (Table. 6).

**Plate.2: Antibacterial activity of *Vernonia cineria* mediated Iron nanoparticles**

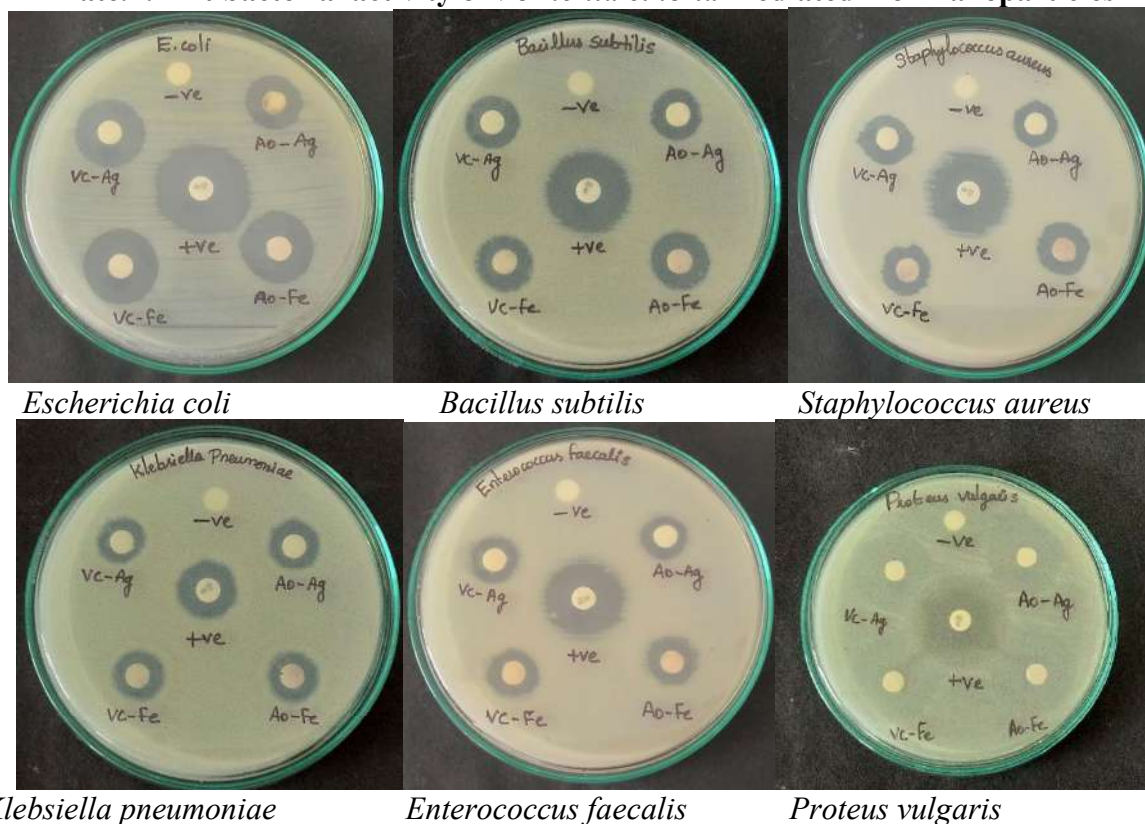
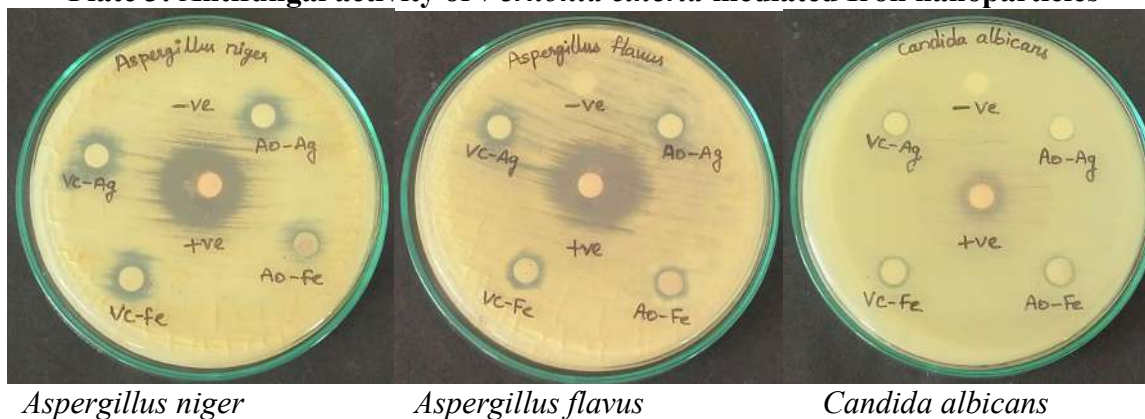


**Table 6: Antifungal activity of *Vernonia cineria* mediated Iron nanoparticles**

| Sample    | <i>A. niger</i> | <i>A. flavus</i> | <i>C. albicans</i> |
|-----------|-----------------|------------------|--------------------|
| Vc- FeNps | 13 mm           | 12 mm            | 10 mm              |
| + ve      | 21 mm           | 21 mm            | 16 mm              |
| - ve      | NZ              | NZ               | NZ                 |

**Plate 3: Antifungal activity of *Vernonia cineria* mediated Iron nanoparticles**



**3.1.11. Photodegradation Activity**

**Table 7: Photodegradation activity of *Vernonia cineria* mediated Iron nanoparticles**

| Time interval |                  | Initial | 20 minutes | 40 minutes | 60 minutes | 80 minutes | 100 minutes | 120 minutes |
|---------------|------------------|---------|------------|------------|------------|------------|-------------|-------------|
| VC-FeNps      | OD at 664 nm     | 0.0243  | 0.0157     | 0.0139     | 0.0092     | 0.0036     | 0.0027      | 0.0016      |
|               | % of degradation | -       | 35%        | 43%        | 62%        | 85%        | 89%         | 93%         |

One of the efficient applications of FeNPs is photodegradation. Photodegradation was noticed in biosynthesized iron nanoparticles at uniform time intervals (0 to 120min) and the absorbance was noticed at 664nm. There were no degradation at the beginning and after 20min the degradation was 35%. Gradually the activity increased to 43% at 40 min and 62% at 60 min. A regular interval of activity was noticed at each 20 min with 85% at 80 min and at 100 min the degradation became lesser than before with a degradation percentage of 89% and 93% at 120 min (Table. 7). Over time, nanoparticles may tend to aggregate, leading to changes in their surface area and exposure to light. Aggregation can affect the reactivity of the nanoparticles and influence their susceptibility to photodegradation. The initial absence of degradation may indicate stable nanoparticle dispersion, while the increase in degradation percentages over time could be attributed to increased aggregation and consequent exposure of aggregated particles to light.

#### 4. Discussion

The biological and environmentally friendly synthesis nano particles process is more efficient than the different physico-chemical procedures that are currently being used. It is possible to influence biological entities such as algae, fungi, bacteria, plants and so on. Using the biological/green technique, which is successful since it does not need the use of costly harmful chemicals or a significant amount of energy (Hussain *et al.*, 2016). This work exhibits the usage of leaf extract from *V. cinerea* for the synthesized of iron nanoparticles. The extract functions as surface stabilizers, capping agents and reducing agents and was successful in demonstrating its application. The reaction that takes place between precursor salts and reducing agents results in the formation of iron nanoparticles. The UV spectra analysis of iron nanoparticles synthesized from *V. cineria* extract revealed absorption peaks at 268nm and 347nm, contrasting with previous findings which reported bands at 216nm and 268nm (Yuvakumar *et al.*, 2011). This discrepancy prompts a deeper examination of the nanoparticles' characteristics. The presence of multiple absorption peaks is suggests a diverse array of iron nanoparticles within the extract. The consistent observation of a peak at 268 nm indicates the fundamental presence of iron nanoparticles. However, the additional peak at 347nm in our study suggests the potential existence of larger or differently shaped iron nanoparticles. Alternatively, it may signify interactions between the iron nanoparticles and other compounds present in the extract, leading to a modification of the absorption spectrum.

The absorption peaks that were detected in the research and the wavelengths that were found in the literature for iron nanoparticles that were synthesized from different plant extracts were 278nm and 216-256nm (Dhuper *et al.*, 2012); 256nm and 277nm (Mohanraj *et al.*, 2014); 325nm and 296nm as well as 259nm and 282nm (Thenmozhi *et al.*, 2014), respectively. This is in good correlation with the study that is currently being conducted. the FTIR spectra of the iron nanoparticles revealed the presence of a number of distinguished functional groups, including carboxylic acids, aromatics and amines. It is quite probable that these functional groups arise from organic molecules that are present in the *V. cineria* extract that was used in the formation of the compound. According to the findings of the earlier investigations, which demonstrated the bands for O-H bonds and C=O bonds (Alencar *et al.*, 2012, Sharma and Bhattacharya, 2005), the bands that were detected are consistent with those findings. The results of the FTIR analysis indicate that the organic functional groups that are present in the plant

extract are likely responsible for stabilizing the iron nanoparticles that were generated from *V. cineria* extract.

The size of the particles that make up iron nanoparticles was determined by using the Deybe-Scherrer equation in conjunction with the two theta value that was obtained from XRD. However, there were a few peaks that were comparable to the peaks that were shown in earlier research that demonstrated the crystallinity of iron nanoparticles (Sun *et al.*, 2006). FeNPs synthesized using extract of leaves of *V. cineria* plant are studied under SEM for morphology, microstructure. It indicates that nanoparticles formed are spherical agglomerated of particle with different size. Jara *et al.* (2024) reported that the iron nanoparticles synthesized with *Vernonia amygdalina* exhibit an irregular morphology and lack a uniform distribution in shape and size. Elemental composition of FeNPs synthesized using *V. cineria* leaves extract was determined by using EDX analysis. It was observed that the percentage of iron is 30.88%, potassium is 26.56% and chlorine is 25.91% are high in FeNPs synthesized *V. cineria*. Palei *et al.* (2023) also reported that EDAX of synthesized silver nanoparticle using the *V. cineria* extracts. Antibacterial assay confirms the efficient antibacterial activity of iron nanoparticles against the pathogens which might be because of the rupture of the membrane caused by the generation of reactive oxygen species, which ultimately results in the death of the cell and were studied earlier by other researchers (Brayner *et al.*, 2006; Jagathesan and Rajiv, 2018). The extract of *V. cineria* was tested for its antibacterial activity against gram-positive and gram-negative pathogens at varying doses, and the results showed that it was effective against both types of infections (Gupta *et al.*, 2003). Similarly the antifungal activity of *V. cineria* derived iron nanoparticles showed a remarkably good activity against *A. niger*, *A. flavus* and *C. albicans* when compared with the positive control. Studies relevant to the current work has been previously done to show the antifungal activity (Parveen *et al.*, 2018). FeNPs were tested for antifungal activity against *C. albicans* and *A. niger* which proved it an effective antifungal activity (Nehra *et al.*, 2018). There is a significant influence on the size of nanoparticles due to the fact that this causes the accumulation of these nanoparticles to be enhanced. As the nanoparticles are above 50nm, it is understood that the nanoparticles are effective in degrading the cytoplasm of the bacteria. Under some circumstances, iron nanoparticles have the potential to function as photocatalysts activity, which would make it easier for organic pollutants to be degraded via the process of photocatalytic reactions. Iron nanoparticles have the ability to create reactive oxygen species (ROS) such as hydroxyl radicals via photoinduced electron transfer processes when they are exposed to light, particularly ultraviolet radiation. In the current study, the percentage of degradation was seen improved gradually from 20 min to 120 min. The percentage of degradation steadily increases from 35% after 20 min to 93% after 120 min. This indicates that the degradation process is ongoing and becomes more pronounced with longer exposure times. The substantial percentage of degradation achieved within the first 100 minutes (up to 89%) indicates the effectiveness of the degradation process under the experimental conditions. Based on the findings of some research, it was determined that a similar sort of activity was taking place, in which the rate of deterioration was high in the first few minutes but slowed down in the later hours (Kiew *et al.*, 2023).

## 5. Conclusion

In this study, we showcased the utilization of *V. cineria* leaf extract for the generation of iron nanoparticles. The extract not only served as a reducing agent but also functioned as surface stabilizers and capping agents, successfully demonstrating its application in nanoparticle synthesis. The formation of FeNPs was confirmed from UV visible spectroscopy, FTIR, XRD, SEM and EDAX analysis. Additionally, antibacterial and antifungal assays demonstrated the efficient activity of the iron nanoparticles against pathogens, consistent with previous studies showed potential antimicrobial properties of synthesized FeNPs *V. cineria* extracts. Moreover, the photodegradation experiments

highlighted the potential of iron nanoparticles to serve as photocatalysts, facilitating the degradation of organic pollutants over time. The gradual increase in degradation percentage observed throughout the experiment underscores the effectiveness of the degradation process, with parallels found in previous research regarding degradation kinetics. The environmentally friendly nature of the synthesis process, coupled with the diverse functional properties of the nanoparticles, holds promise for various applications in fields such as biomedicine, environmental remediation and catalysis. Further research and development in this area are warranted to explore the full potential of green synthesis techniques and their applications in sustainable nanotechnology.

## 6. References

1. Alencar, W.S., Acayanka, E., Lima, E.C., Royer, B., de Souza, F.E., Lameira, J., Alves, C.N. (2012). Application of *Mangifera indica* (mango) seeds as a biosorbent for removal of Victazol Orange 3R dye from aqueous solution and study of the biosorption mechanism. *Chemical Engineering Journal*, 209:577–588.
2. Azim, Z., Singh, N. B., Khare, S., Singh, A., Amist, N., & Yadav, R. K. (2022). Green synthesis of zinc oxide nanoparticles using *Vernonia cinerea* leaf extract and evaluation as nano-nutrient on the growth and development of tomato seedling. *Plant Nano Biology*, 2, 100011.
3. Brayner, R., Ferrari-Iliou, R., Brivois, N., Djediat, S., Benedetti, M.F & Fievet, F., 2006. Toxicological impact studies based on *Escherichia coli* bacteria in ultrafine ZnO nanoparticles colloidal medium. *Nano Lett.* 6, 866–870.
4. Chauhan, H., Tanweer, M. S., & Alam, M. (2023). Efficient removal of cationic and anionic dyes from synthetic and real wastewater by plant-mediated nickel nanoparticles. *Oriental Journal of Chemistry*, 39(3).
5. Dhuper, S., Panda, D., & Nayak, P.L. (2012). Green synthesis and characterization of zero valent iron nanoparticles from the leaf extract of *Mangifera Indica*. *Nano Trends: A Journal of Nanotechnology and Its Applications*, 13:16-22.
6. Dinali, R., Ebrahiminezhad, A., Manley-Harris, M., Ghasemi, Y., & Berenjian, A. (2017). Magnetic immobilization of bacteria using iron oxide nanoparticles. *Biotechnology Letters*. <https://doi.org/10.1007/s10529-017-2477-0>.
7. Ebrahiminezhad, A., Barzegar, Y., Ghasemi, Y., & Berenjian, A. (2016). Green synthesis and characterization of silver nanoparticles using *Alcea rosea* flower extract as a new generation of antimicrobials. *Chemical Industry and Chemical Engineering Quarterly*, 0, 2.
8. Gupta, M., Mazumder, U.K., Manikandan, L., Haldar, P.K., Bhattacharya, S., & Kandar, C.C. (2003). Antibacterial activity of *Vernonia cinerea*. *Fitoterapia*, 74(1-2), 148-150.
9. Hussain, I., Singh, N.B., Singh, A., & Singh, H. (2017). Allelopathic potential of sesame plant leachate against *Cyperus rotundus* L. *Annals of Agrarian Science* 15, 141–147.
10. Jagathesan, G., & Rajiv, P. (2018). Biosynthesis and characterization of iron oxide nanoparticles using *Eichhornia crassipes* leaf extract and assessing their antibacterial activity. *Biocatalysis and agricultural biotechnology*, 13, 90-94.
11. Jara, Y.S., Mekiso, T.T. & Washe, A.P (2024). Highly efficient catalytic degradation of organic dyes using iron nanoparticles synthesized with *Vernonia Amygdalina* leaf extract. *Scientific report*, 14: 6997.
12. Kiew, P.L., Fauzi, N.A. M., Firdiani, S.A., Lam, M.K., Tan, L.S., & Yeoh, W.M. (2023). Iron oxide nanoparticles derived from *Chlorella vulgaris* extract: Characterization and crystal violet photodegradation studies. *Progress in Energy and Environment*, 1-10.



13. Makarov, V., Love, A., Sinitsyna, O., Makarova, S., Yaminsky, I., Taliansky, M., & Kalinina, N. (2014). "Green" nanotechnologies: Synthesis of metal nanoparticles using plants. *Acta Naturae*, 6(1(20)), 35–44.
14. Mohanraj, S., Kodhaiyolii, S., Rengasamy, M., & Pugalenti, V. (2014). Green synthesized iron oxide nanoparticles effect on fermentative hydrogen production by *Clostridium acetobutylicum*. *Applied Biochemistry and Biotechnology* 173:318–331.
15. Nehra, P., Chauhan, R., Garg, N., & Verma, K. (2018). Antibacterial and antifungal activity of chitosan coated iron oxide nanoparticles. *British Journal of Biomedical Science*, 75(1), 13–18.
16. Palei, N.N., Krishnan, N., Jayaraman, R., Reddy, S.H., Balaji, A., Samanta, M.K., & Mohanta, B. (2023). Green Synthesis of Silver Nanoparticles of *Vernonia cinerea* Leaf Extract and their *In vitro* Cytotoxicity Activity against Neuroblastoma SHSY-5Y Cell Lines, Antimicrobial and Antioxidant Studies. *Recent Pat Nanotechnol.*17(3):270-280.
17. Parveen, S., Wani, A.H., Shah, M.A., Devi, H.S., Bhat, M.Y., & Koka, J.A. (2018). Preparation, characterization and antifungal activity of iron oxide nanoparticles. *Microbial pathogenesis*, 115, 287-292.
18. Ramaswamy, U., Mukundan, D., Sreekumar, A., & Mani, V. (2015). Green synthesis and characterization of silver nanoparticles using aqueous whole plant extract of *Vernonia cinerea* L. and its biological activities. *Materials Today: Proceedings*, 2(9), 4600-4608.
19. Sharma, A., & Bhattacharyya, K.G. (2005). *Azadirachta Indica* (Neem) leaf powder as a biosorbent for removal of Cd(II) from aqueous medium. *Journal of Hazardous Materials*, 125:102-112.
20. Singh, L., Antil, R., & Dahiya, P. (2021). Antimicrobial and antioxidant potential of *Vernonia cinerea* extract coated AuNPs. *Indian Journal of Microbiology*, 61, 506-518.
21. Sun, Y.P., Li, X.Q., Cao, J., Zhang, W.X., & Wang, H.P. (2006). Characterization of zero-valent iron nanoparticles. *Advances in Colloid and Interface Science*, 120(1-3), 47-56.
22. Thenmozhi, B., Suryakiran, S., Sudha, R., & Revathy, B. (2014). Green synthesis and comparative study of silver and iron nanoparticle from leaf extract. *International Journal of Institutional Pharmacy and Life Sciences* 4:5-12.
23. Yuvakkumar, R., Elango, V., Rajendran, V., & Kannan, N. (2011). Preparation and characterization of zero valent iron nanoparticles. *Digest Journal of Nanomaterials and Biostructures*, 6(4), 1771-1776.